Clear detection of dusty torus signatures in a weak-line radio galaxy: the case of PKS 0043−42

C. Ramos Almeida,[1]* D. Dicken,[2] C. Tadhunter,[1] A. Asensio Ramos,[3,4] K. J. Inskip,[5] M. J. Hardcastle[6] and B. Mingo[6]

[1]*Department of Physics and Astronomy, University of Sheffield, Sheffield, S3 7RH*
[2]*Department of Physics and Astronomy, Rochester Institute of Technology, 84 Lomb Memorial Drive, Rochester NY 14623, USA*
[3]*Instituto de Astrofísica de Canarias (IAC), C/Vía Láctea, s/n, E-38205, La Laguna, Tenerife, Spain*
[4]*Departamento de Astrofísica, Universidad de La Laguna, E-38205, La Laguna, Tenerife, Spain*
[5]*Max-Planck-Institut für Astronomie, Königstuhl 17, D-69117 Heidelberg, Germany*
[6]*School of Physics, Astronomy and Mathematics, University of Hertfordshire, College Lane, Hatfield, Hertfordshire AL10 9AB*

ABSTRACT

We report the clearest detection to date of dusty torus signatures in a weak-line radio galaxy (WLRG). The deep *Spitzer* InfraRed Spectrograph (IRS) rest-frame mid-infrared (MIR) spectrum of the WLRG PKS 0043−42 ($z = 0.116$) shows a clear spectral turnover at $\lambda \gtrsim 20\,\mu s$ suggestive of warm dust, as well as a 9.7-μm silicate absorption feature. In addition, the hard X-ray results, based on *Chandra* data, strongly support a picture in which PKS 0043−42 has a torus and accretion disc more typical of strong-line radio galaxies (SLRGs). The MIR and X-ray spectra are markedly different from those of other WLRGs at similar redshifts, and here we show that the former can be successfully fitted with clumpy torus models with parameters characteristic of Type-2 AGN tori: close to edge-on ($i = 74°$) and relatively broad ($\sigma = 60°$), with an outer radius of 2 pc, $N_H = 1.6 \pm^{0.2}_{0.1} \times 10^{23}\,\mathrm{cm}^{-2}$, and AGN bolometric luminosity $L_\mathrm{bol}^\mathrm{AGN} = 1.6 \pm^{0.2}_{0.1} \times 10^{44}\,\mathrm{erg\,s}^{-1}$. The presence of a compact torus in PKS 0043−42 provides evidence that this WLRG is fuelled by cold, rather than hot, gas accretion. We suggest that WLRGs are a diverse population, and PKS 0043−42 may represent a type of radio galaxy in which the AGN activity has been recently re-triggered as a consequence of intermittent gas supply, or in which the covering factor of the narrow-line region (NLR) clouds is relatively low.

Key words: galaxies: active – galaxies: individual: PKS 0043−42 – galaxies: nuclei – infrared: galaxies – X-rays: galaxies.

1 INTRODUCTION

Most powerful radio galaxies (PRGs) can be classified as narrow- and broad-line radio galaxies/quasars (NLRGs, BLRGs/QSOs) on the basis of their spectral features. The unified model for active galactic nuclei (AGN; Antonucci 1993; Urry & Padovani 1995), proposes the existence of a pc-scale obscuring toroidal structure to account for the observed differences between their spectra. However, there is also a third class, the WLRGs (also known as low-excitation galaxies, LEGs), whose optical spectra are dominated by the stellar continua of the host galaxies (Laing et al. 1994; Tadhunter et al. 1998) without the prominent emission lines characteristic of NLRGs and BLRGs (which can be grouped as SLRGs, or alternatively, high-excitation galaxies, HEGs).

The nature of the physical parameters which lead to the division between SLRGs and WLRGs still remains unclear. Previous studies failed to explain the differences between the two types as due to different or time-varying accretion rates (Ghisellini & Celotti 2001). An alternative interpretation is that SLRGs are powered by cold gas accretion, while WLRGs are fuelled by accretion of hot gas provided by the reservoir of their X-ray gaseous coronae (Allen et al. 2006; Best et al. 2006; Hardcastle, Evans & Croston 2007; Balmaverde, Baldi & Capetti 2008; Buttiglione et al. 2010). The high temperatures of the hot gas would prevent the formation of the 'cold' structures (e.g. the broad-line region and the torus). This hypothesis explains the fact that WLRGs do not normally show the high level of X-ray absorption expected of a molecular torus (Hardcastle, Evans & Croston 2009).

SLRGs are almost invariably associated with Fanaroff–Riley II sources (FRII). On the other hand, while most WLRGs show Fanaroff–Riley I (FRI) radio morphologies, some are classified as

*E-mail: C.Ramos@sheffield.ac.uk

FRIIs (Laing et al. 1994). Evidence for nuclear warm dust emission has been found in the MIR for FRII/SLRGs (Ogle, Whysong & Antonucci 2006; van der Wolk et al. 2010) and, to a lesser extent, for a few FRI and FRII WLRGs (Leipski et al. 2009; van der Wolk et al. 2010). However, none of the WLRGs so far studied has provided definitive evidence for a warm compact obscuring region e.g. in the form of a spectral turnover at ∼20 μm and a clear silicate absorption feature. This lack of conclusive detection of torus signatures in previous studies may be due to contamination of the MIR data by stellar photospheric and starburst-heated dust components, which generally produces a broad minimum in the 8–10 μm range and can be confused with a silicate absorption feature. Strong PAH (in particular the 8.2- and 11.3-μm features) and non-thermal emission from the synchrotron-emitting core sources can also mask the torus signatures. Based on extrapolation of the radio core data, the latter emission appears particularly important in WLRGs at MIR wavelengths (Dicken et al. 2008; van der Wolk et al. 2010). All of these diluting components need to be accurately subtracted before the presence of warm dust can be deduced.

At optical wavelengths the galaxy PKS 0043−42 is classified as a WLRG at redshift $z = 0.116$ (Tadhunter et al. 1993), whereas at radio wavelengths it shows a clear FRII morphology (Morganti, Killeen & Tadhunter 1993; Morganti et al. 1999). According to Tadhunter et al. (1998), the WLRGs are defined as a group of galaxies with [O III] λ5007 emission line equivalent widths below 10 Å. PKS 0043−42 not only fulfills this criterion, but also has an [O III] λ5007 luminosity a factor of 10 lower than those of the general population of SLRGs at similar redshifts and radio powers ($L_{\mathrm{[O III]}} = 5 \times 10^{40}$ erg s^{-1}; Tadhunter et al. 1998; Dicken et al. 2009), as well as line ratios indicating a low ionization state (e.g. [O III] λ5007/[O II] λ3727 < 1; Tadhunter et al. 1998; Lewis, Eracleous & Sambruna 2003). The galaxy is at the centre of a group or cluster, and from NIR imaging, Inskip et al. (2010) reported a central isophotal twist and an excess of emission along the NS direction. They claimed that both are likely to be associated either with the presence of a dust lane, or with the apparent interaction with the companion object ∼15 kpc to the North. However, the deep optical image presented in Ramos Almeida et al. (2011) does not reveal any dust features in PKS 0043−42, but appears instead to confirm the presence of the bridge with the companion galaxy.

In this study we report the detection of torus signatures in the MIR and X-ray spectra of the WLRG PKS 0043−42. In the following sections we describe the observations, the SED modelling, the main results and their implications. Throughout this paper we assume a cosmology with $H_0 = 73$ km s^{-1} Mpc^{-1}; $\Omega_{\mathrm{m}} = 0.27$, and $\Omega_{\Lambda} = 0.73$, which provides a luminosity distance of 516 Mpc for PKS 0043−42 (from the NASA/IPAC Extragalactic Data base; NED).

2 OBSERVATIONS

2.1 *Spitzer* observations

MIR spectroscopic observations of PKS 0043−42 were obtained using the IRS instrument (Houck et al. 2004) on the *Spitzer* satellite on 2008 December 12 under the programme 2JYSPEC/50558 (PI: C. Tadhunter). The observations were made in staring mode using the two low-resolution ($R \sim 60–120$) IRS modules: the short-low (SL; 5.2–14.5 μm) and the long-low (LL; 14–38 μm). The slitwidths are 3.7 and 10.7 arcsec for the SL and LL modules, respectively. Four cycles of 60-s exposures were taken in each of the two SL modules, and two cycles of 120 s for the LL modules. The data were downloaded from the *Spitzer* archive in basic calibrated data (BCD)

product form, processed with the S18.7.0 pipeline, and reduced and extracted using the SMART v.8.1.2 program developed by the IRS Team at Cornell University (Higdon et al. 2004; Lebouteiller et al. 2010). In extracting the fluxes we used the optimal extraction function which uses a supersampled PSF and weights the extracted spectra using the signal-to-noise ratio of each pixel (Lebouteiller et al. 2010). Note that the IRS pipeline automatically accounts for variable slit losses with wavelength. For each cycle the nod positions were subtracted in order to perform background subtraction on the image, as well as to counteract intrinsic sensitivity variations across the detector. For a more detailed description of the observations and data reduction, see Dicken et al. (in preparation). The two resulting spectra were then combined to produce the final spectrum shown in Fig. 1. The absolute uncertainty in the flux calibration at the 1σ level is ∼15 per cent for the SL and LL data, whereas for the spectral shape it is much less than that (Decin et al. 2004; Roellig et al. 2004). We have scaled the observed IRS spectrum to the Multiband Imaging Photometer for *Spitzer* (MIPS) 24 μm flux (11.1 ± 0.2 mJy; Dicken et al. 2008), obtained using a 15-arcsec aperture. The discrepancy between the IRS and MIPS fluxes at 24 μm is only ∼10 per cent.

In addition to the IRS spectrum, we compiled the following.

(1) An NIR upper limit flux of 0.45 ± 0.02 mJy derived from the GALFIT analysis of K_s-band SofI images presented in Inskip et al. (2010). This value corresponds to an unresolved component of 0.93 arcsec of FWHM.

(2) An MIPS 70 μm flux of 9.9 ± 3.0 mJy from Dicken et al. (2008). For the analysis performed here, we consider this flux an upper limit, because at this wavelength and with the aperture employed for calculating it (24 arcsec; Dicken et al. 2008) the emission is likely to be dominated by dust heated by stars and/or AGN heated dust in the NLR. In Fig. 2 we present the MIPS images of PKS 0043−42 at 24 and 70 μm (from the 2-Jy webpage http://2jy.extragalactic.info and described in Dicken et al. 2008), to show the difference in the signal-to-noise level of the two detections.
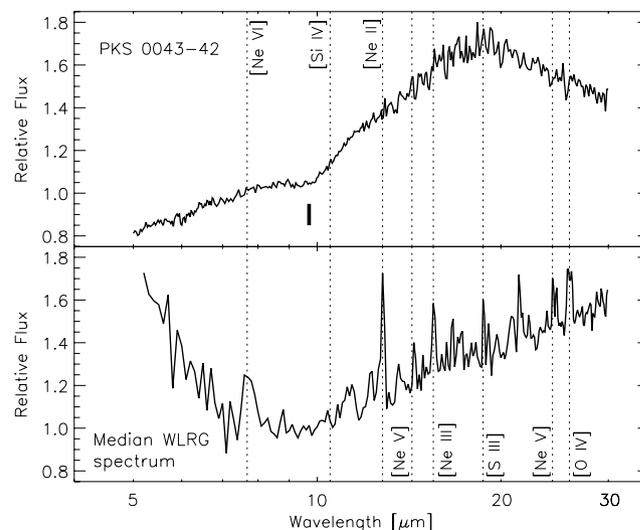
Figure 1. Low-resolution IRS rest-frame spectrum of PKS 0043−42 in relative F_ν units (top). Note the emission bump peaking at ∼20 μm and the 9.7 μm silicate feature in absorption (short vertical line), both characteristic of a dusty torus. The spectral features and shape are different from those of the 2-Jy median WLRG spectrum (bottom). Typical AGN emission lines are labeled.
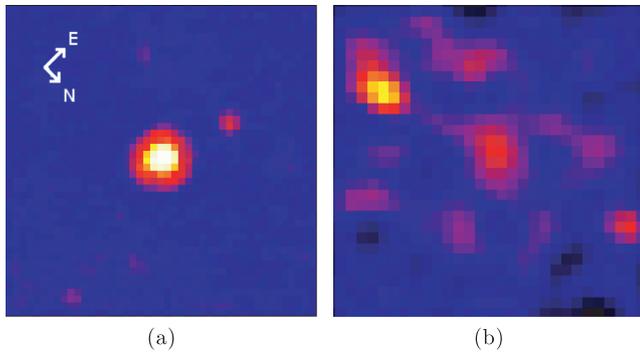
Figure 2. MIPS 24 μm (a) and 70 μm (b) images (the latter is smoothed using a box of the size of 2 pixels) of PKS 0043−42. Panels are 110 arcsec each side.

(3) High angular resolution radio core fluxes of 4.5 ± 0.8 mJy at 2.3 GHz (13 cm) from Morganti et al. (1997), and 1.4 ± 0.3 mJy at ∼15 GHz (2 cm) from Dicken et al. (2008).

The IR-to-radio SED of PKS 0043−42 is shown in Fig. 3. From the radio core data points it becomes clear that, for any reasonable extrapolation of the radio core spectrum, non-thermal emission does not contribute significantly to the MIR emission of this galaxy. By looking at the high-resolution radio maps shown in Morganti et al. (1997) we can also rule out significant contamination (by extended emission from the radio lobes) of the IRS data (maximum slitwidth of 4.46 arcsec).

The MIR spectrum of PKS 0043−42 (Fig. 1) shows a clear 9.7 μm silicate absorption feature and a spectral turnover at $\lambda \gtrsim 20$ μm. These are the most convincing detections of torus signatures to date in a WLRG. We can quantify the 9.7 μm silicate feature in terms of its strength, defined as $\tau_{9.7}^{\mathrm{app}} = \ln(F_{\mathrm{cont}}) - \ln(F_{\mathrm{core}})$. We calculate F_{cont} using a cubic spline interpolation in logarithmic space over two intervals at shorter and longer wavelengths than the region covered by the silicate feature to fit the continuum and F_{core} allowing the peak wavelength to vary, following Sirocky et al. (2008). By doing this, we find $\tau_{9.7}^{\mathrm{app}} = 0.2$. The lack of strong emission lines in the IRS spectrum is also remarkable.
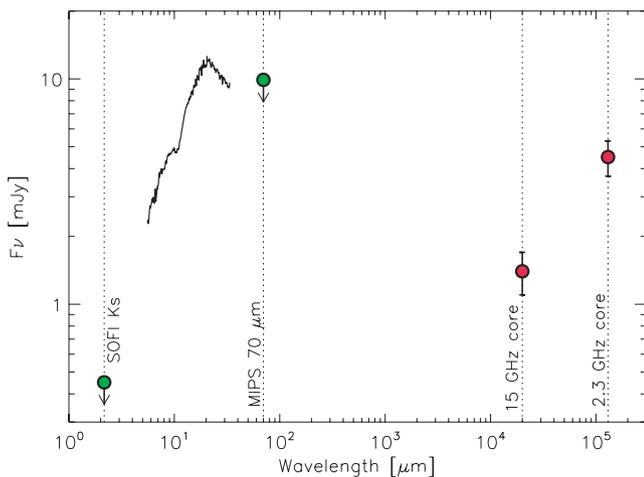
All of these features, as well as the spectral shape, are markedly different from those of the median spectrum shown in the bottom panel of Fig. 1, which was constructed using IRS data for all the WLRGs in the 2-Jy sample with redshift $0.05 < z < 0.15$ (excluding PKS 0034−01, which is affected by saturation problems), and is representative of WLRGs at similar redshifts to PKS 0043−42 (see also Leipski et al. 2009). At short wavelengths, this average WLRG spectrum shows a blue spectral slope, which corresponds to the tail of the photospheric emission from the stars in the host galaxy. At longer wavelengths, the continuum appears relatively flat, although rising slowly with wavelength. This shape is likely produced by a combination of non-thermal emission and extended dust emission heated by stars (Leipski et al. 2009). As mentioned in Section 1, there is evidence for strong synchrotron contamination at MIR and far-infrared wavelengths in many WLRGs, based on their IR-to-radio SEDs (Dicken et al. 2008; van der Wolk et al. 2010). Finally, emission lines such as [Ne II] λ12.8, [Ne III] λ15.5 and [O IV] λ25.9 μm are also detected in the median WLRG spectrum.

2.2 *Chandra* observations

PKS 0043−42 was observed with *Chandra* on 2009 February 05 (obsid 10319) as a part of a systematic programme of *Chandra* observations of the complete steep-spectrum 2-Jy sample in the redshift range $0.05 < z < 0.2$ (details of all the observations, including further results from the observation of PKS 0043−42, will be presented by Mingo et al., in preparation). The time on source was 18.4 ks. X-ray emission from the nucleus was clearly detected, at the level of ∼150 counts in the 0.5-5.0 keV energy band, and we extracted an X-ray spectrum of the nucleus in the manner described by Hardcastle, Evans & Croston (2006). This spectrum is shown in Fig. 4.

The spectrum is clearly different from what is usually seen in WLRGs (Hardcastle et al. 2006), namely a single power law with little or no intrinsic absorption: a peak at high energies indicates the need for an absorbed component in the model. Therefore, we fitted the standard model for narrow-line radio galaxies, consisting of two power laws, one with absorption fixed at the Galactic value ($N_{\mathrm{H}} = 2.7 \times 10^{20}$ cm^{-2}), and one with an additional free variable

Figure 3. SED of PKS 0043−42 including the NIR K_s-band upper limit, the IRS observed spectrum scaled to the MIPS 24 μm point, the MIPS 70 μm upper limit and the 15- and 2.3-GHz radio core fluxes. The latter indicate that non-thermal emission from the radio core does not contribute significantly to the MIR emission.
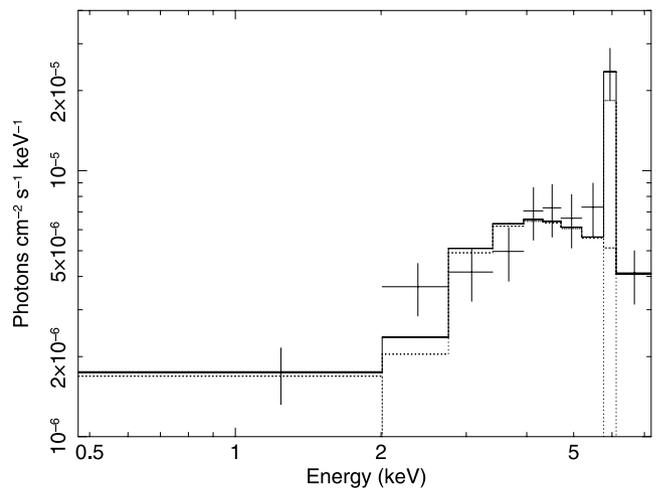
Figure 4. *Chandra* ACIS-S spectrum of PKS 0043−42. The model consists of local absorption, intrinsic absorption, two power laws and a Gaussian to account for the Fe emission line. The presence of this emission line is associated with accreting structures, which are typically seen in NLRGs, but have not been unequivocally observed in WLRGs before.

© 2011 The Authors, MNRAS **413,** 2358–2364
Monthly Notices of the Royal Astronomical Society © 2011 RAS

absorption. Because of the small number of counts in the spectrum, we fixed the photon indices of the unabsorbed and absorbed power laws to the values used by Hardcastle et al. (2006), i.e. 2.0 and 1.7, respectively. A fit of this model showed strong residuals at 6–7 keV, which could not be removed by allowing the photon index of the absorbed power law to vary; a good fit could only be obtained with the addition of a narrow Gaussian feature with $E = 6.47^{+0.39}_{-0.04}$ keV, consistent with being an Fe $K\alpha$ line (indicative of the presence of an accretion disc). The best-fitting absorption column density in this model was $1.20^{+0.55}_{-0.36} \times 10^{23}$ cm^{-2} and the unabsorbed 2–10 keV luminosity of the heavily absorbed power-law component was $1.83^{+0.10}_{-0.12} \times 10^{43}$ erg s^{-1}. The high obscuring column density and the clearly detected iron feature are both very commonly seen in NLRGs, but have not so far been seen in bona fide WLRGs (e.g. Hardcastle et al. 2009).

In addition, the X-ray luminosity lies in the region populated by NLRGs on a plot of absorbed X-ray luminosity against low-frequency radio luminosity (fig. 3 of Hardcastle et al. 2009), as well as on the correlation between the 15-μm luminosity (5.8 × 10^{43} erg s^{-1}, as measured from the IRS spectrum) and the unabsorbed X-ray luminosity (fig. 10 of Hardcastle et al. 2009). Thus, the X-ray results strongly support the picture in which PKS 0043−42, while spectroscopically classified as a WLRG, has a torus and accretion disc more typical of an NLRG.

3 SED MODELLING

Our aim is to investigate whether or not the IR SED of PKS 0043−42 can be reproduced by torus models. The IR range (and particularly the MIR; 5–30 μm) is key for setting constraints on the torus models, since the reprocessed radiation from the dust in the torus is re-emitted in this range. Recent ground-based MIR imaging (see e.g. Packham et al. 2005; Radomski et al. 2008) and interferometric observations of nearby AGN (e.g. Jaffe et al. 2004; Tristram et al. 2007) reveal that the torus size is likely restricted to a few parsecs – much smaller than the resolution of the IRS spectra. Thus, large aperture data such as those employed here may potentially be contaminated by (i) photospheric emission from stars, (ii) extended dust emission heated by stars and/or the AGN, and (iii) non-thermal emission. First, the optical spectrum and the lack of polycyclic aromatic hydrocarbons (PAHs) in the MIR suggest that star formation is not important in PKS 0043−42. Second, extended dust emission from the NLR cannot be a substantial source of contamination either if we consider the low emission line luminosity measured for this galaxy (Tadhunter et al. 1998; Dicken et al. 2009). Finally, in Section 2.1 we have shown that the non-thermal emission from the radio core and the lobes does not contribute significantly to the MIR

emission of this object. Thus, the dominant contribution to our IR data must be nuclear dust heated by the AGN.

The clumpy dusty torus models of Nenkova, Ivezic & Moshe (2002) hold that the dust surrounding the central engine of an AGN is distributed in clumps, instead of homogeneously filling the torus volume. These clumps are distributed with a radial extent $Y = R_{\rm o}/R_{\rm d}$, where $R_{\rm o}$ and $R_{\rm d}$ are the outer and inner radius of the toroidal distribution, respectively. The clumpy data base now contains 5×10^6 models, calculated for a fine grid of model parameters. To take into account the inherent degeneracy between these parameters when fitting observables, here we use an updated version of the Bayesian inference tool BAYESCLUMPY, developed by Asensio Ramos & Ramos Almeida (2009). BAYESCLUMPY applies interpolation methods that are able to derive models for different combinations of the clumpy model parameters even if they are not present in the original data base. For an example of the use of clumpy model fitting to IR SEDs using BAYESCLUMPY, see Ramos Almeida et al. (2009). The new version of BAYESCLUMPY allows the fitting of photometric and spectroscopic data simultaneously. Thus, here we use an interpolated version of the clumpy models of Nenkova et al. (2008a,b) including the corrections for the previously erroneous AGN scaling factor (see erratum by Nenkova et al. 2010).

The result of the SED fitting are the posterior/probability distributions for the six free parameters that describe the models (see Table 1 for a description of the parameters) and the vertical shift (Fig. 5). In addition, we can translate these results into corresponding spectra (Fig. 6). Thus, the maximum-a-posteriori (MAP) spectral energy distribution (SED) represent the 'best fit' to the data (solid line), i.e. the combination of parameters that maximizes the overall probability/posterior distribution. The dashed line is the SED obtained using the median value of the probability distribution of each parameter, and the shaded region in Fig. 6 indicates the range of models compatible with all the possible combinations of parameters within their 68 per cent confidence intervals around the medians. Fig. 6 shows how well the clumpy models fit the observational data. Both the 20-μm turnover and the silicate feature in weak absorption are reproduced by the MAP and the median models.

4 RESULTS

The more information provided by the IR SED, the better the probability distributions are constrained. From Fig. 5 it is clear that the IR data of PKS 0043−42 constrain the six parameters well (two last columns of Table 1). Thus, the IR emission of this radio galaxy can be reproduced by a broad clumpy torus (torus width of $\sigma = 60°$) with an average number of clouds $N_0 = 5$ along the radial equatorial direction, a radial extent $Y = 12$ and close to edge-on inclination

Table 1. Clumpy model parameters. Columns 1 and 2 give the parameter description and abbreviation used in the text. Column 3 shows the input ranges considered for the fit (i.e. the lower and upper limits of the uniform priors). Finally, columns 4 and 5 list the resulting median and mode values of the resulting probability distributions resulting from the fit (Fig. 5).

Parameter	Abbreviation	Interval	Fitting results	
			Median	Mode
Width of the angular distribution of clouds	σ	[15°, 75°]	$60°\pm^{6°}_{13°}$	68°
Radial extent of the torus ($R_{\rm o}/R_{\rm d}$)	Y	[5, 30]	12 ± 1	12
Number of clouds along the radial equatorial direction	N_0	[1, 15]	5 ± 1	5
Power-law index of the radial density profile	q	[0, 3]	$0.3 \pm^{0.3}_{0.2}$	0.3
Inclination angle of the torus	i	[0°, 90°]	$74° \pm 8°$	75°
Optical depth per single cloud	τ_V	[10, 200]	$18 \pm^5_3$	18
A_V produced by the torus along the LOS	$A_V^{\rm LOS}$	...	$84 \pm^{11}_7$ mag	79 mag
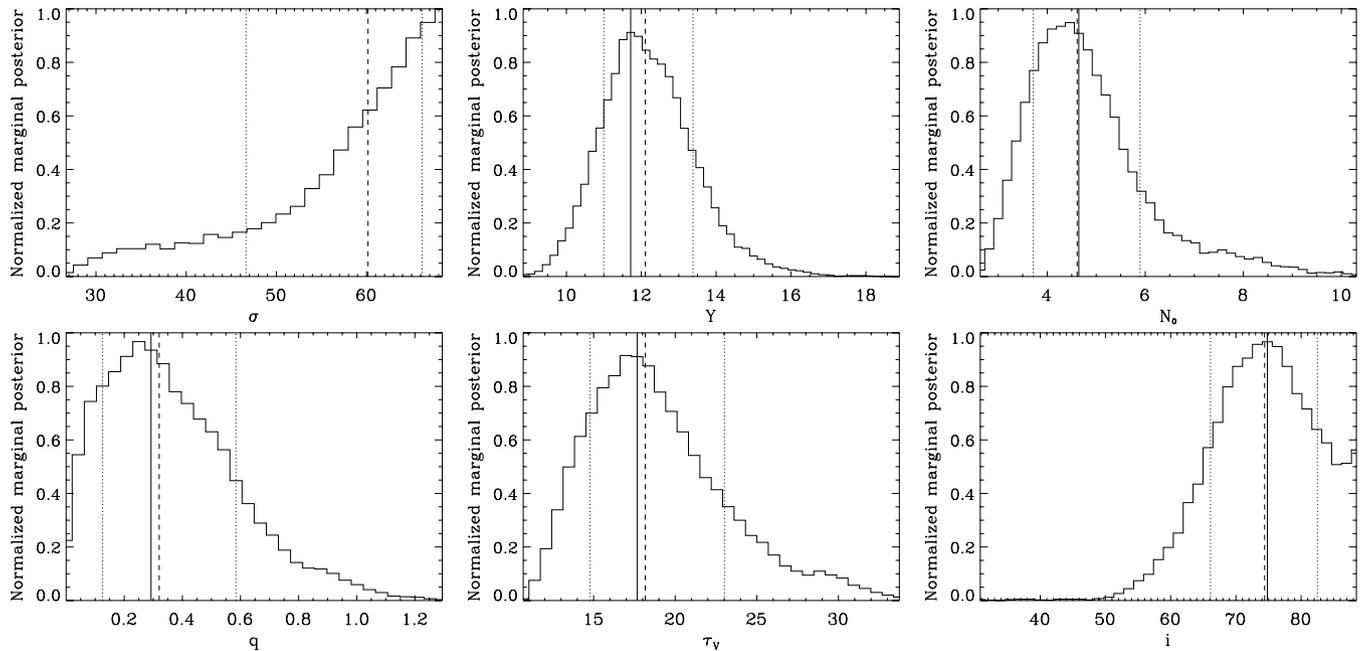
Figure 5. Probability distributions of the free parameters that describe the clumpy models resulting from the fit of PKS 0043−42. The vertical shift has been marginalized. Solid and dashed vertical lines represent the MAP and the median values of each distribution respectively, and the dotted vertical lines indicate the 68 per cent confidence level for each parameter around the median.

($i = 74°$). The optical extinction produced by the torus along the line-of-sight (LOS) is $A_V^{\rm LOS} = 1.086\, N_0\, \tau_V\, e^{(-(i-90)^2/\sigma^2)} = 84$ mag.

The clumpy model fits yield the intrinsic bolometric luminosity of the AGN by means of the vertical shift applied to match the observational data points: $L_{\rm bol}^{\rm MIR} = 1.6\,{}^{+0.2}_{-0.1} \times 10^{44}$ erg s^{-1}. This value can be direct ly compared with the unabsorbed 2–10 keV bolometric luminosity measured from *Chandra* hard X-ray observations by using a bolometric correction factor of 20 (Elvis et al. 1994): $L_{\rm bol}^X = 3.7 \times 10^{44}$ erg s^{-1} (see Section 2.2). Thus, we find $L_{\rm bol}^X \sim 2 \times L_{\rm bol}^{\rm MIR}$, which is consistent within the uncertainties. In fact, these luminosity values are typical of SLRGs (Hardcastle et al. 2009), and both the MIR (24 and 70 μm) and [O III] λ5007 Å luminosities reported in Dicken et al. (2009) for PKS 0043−42 are at the upper end of the WLRG range in the 2-Jy sample.

The outer size of the torus ($R_o = Y R_d$) scales with the AGN bolometric luminosity, so assuming a dust sublimation temperature of 1500 K, $R_o = 0.4 Y (L_{\rm bol}^{\rm MIR}/10^{45})^{0.5}$ pc. Considering the median value of $Y = 12$ determined from our fit, we find that the torus in PKS 0043−42 has an outer extent of $R_o \sim 2$ pc. This value is consistent with interferometric observations of nearby AGN, which indicate that the torus emission only extends out to 1–2 pc (see e.g. Jaffe et al. 2004; Tristram et al. 2007).

Using the $A_V^{\rm LOS}$ value reported in Table 1 we can derive the column density using the Galactic dust-to-gas ratio ($N_{\rm H}^{\rm LOS} = 1.9 \times 10^{21}\, A_V^{\rm LOS}$; Bohlin, Savage & Drake 1978). This gives a value of $N_{\rm H}^{\rm LOS} = 1.6\,{}^{+0.2}_{-0.1} \times 10^{23}$ cm^{-2}, which is similar to that measured from the *Chandra* X-ray observations ($N_{\rm H}^{\rm X-rays} = 1.2\,{}^{+0.5}_{-0.4} \times 10^{23}$ cm^{-2}; Section 2.2). This indicates that the columns of material implied in the X-ray absorption are comparable to those inferred from our IR data. Thus, dust-free gas absorption (i.e. gas located inside R_d) does not appear to be important here. This result contrasts with the findings for Seyfert galaxies and QSOs reported by Maiolino et al. (2001), who claimed that the absorption of the nuclear region in these objects, as derived from optical and IR broad lines, is generally much lower than that obtained from the gaseous column
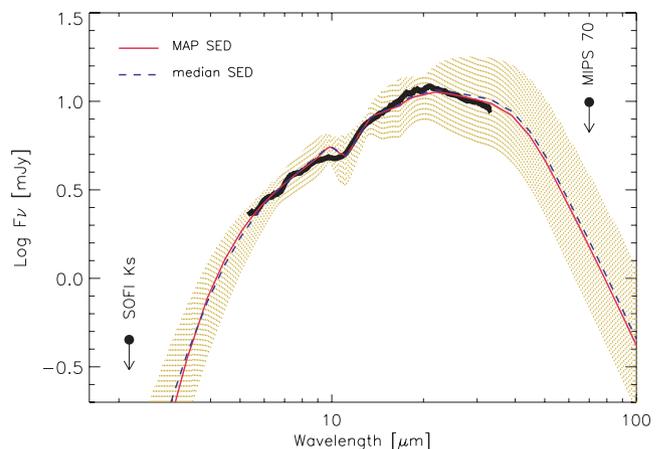
Figure 6. Fit of the observed IRS spectrum (thick solid line spanning 5–30 μm) and the SOFI K_s and MIPS 70-μm data. Dashed and solid lines correspond to the median and MAP models, respectively. The shaded region indicates the range of models compatible with all the possible combinations of the parameters within their 68 per cent confidence intervals around the medians.

density deduced from the X-rays, if a standard Galactic dust-to-gas ratio is assumed.

5 DISCUSSION AND CONCLUSIONS

Based on our analysis, we conclude that the MIR emission of PKS 0043−42 can be accounted for by a clumpy dusty torus with the characteristics shown in Table 1. The derived model parameters are compatible with those obtained for Type-2 AGN of similar AGN bolometric luminosities (see e.g. Ramos Almeida et al. 2009). The presence of a torus is also confirmed by hard X-ray *Chandra* observations, which show clear evidence for a heavily absorbed AGN nucleus and a strong iron $K\alpha$ line, which are commonly seen in

SLRGs but not in WLRGs (Section 2.2). Indeed, its AGN bolometric luminosity ($L^X_{\rm bol} = 3.7 \times 10^{44}$ erg s^{-1}) indicates the presence of a moderately luminous hidden AGN. It has been proposed that the properties of WLRGs, whose spectra lack prominent emission lines, are the result of the Bondi accretion of hot gas, which prevents the formation of the classical AGN structures such as the torus or the BLR. However, the presence of a compact dusty torus and accretion disc signatures in PKS 0043−42 provides evidence that this WLRG is fuelled by cold, rather than hot, gas accretion.

One question that arises from our result is: if there is a moderately luminous AGN heating a nearly edge-on dusty torus, why are we not detecting the strong, high equivalent width emission lines characteristic of NLRGs at either optical or MIR wavelengths? It is important to emphasize that, although PKS 0043−42 falls close to the correlation between MIR and [O III] luminosity for 2-Jy radio galaxies, its [O III] luminosity is a factor of 10 lower than that of SLRGs at similar redshifts and radio powers (Tadhunter et al. 1998), leading to the low equivalent width of the emission lines at optical wavelengths. On the other hand, in the case of the MIR spectrum, the non-linearity of the correlation between emission line and MIR luminosity (Dicken et al. 2009, 2010) will naturally lead to the objects at the lower-luminosity end of the correlation having smaller emission line equivalent widths than their higher-luminosity counterparts. In the case of PKS 0043−42, this effect is exacerbated by the fact that it lies slightly above (∼0.3 dex, or a factor of 2) the $L_{24\,\mu m}$ versus $L_{\rm [O III]}$ correlation, potentially making the MIR fine structure lines even harder to detect against the thermal continuum.

Note that the position of PKS 0043−42 above the $L_{24\,\mu m}$ versus $L_{\rm [O III]}$ correlation can be explained if the dusty torus structure emitting the MIR continuum has a relatively large covering factor compared with the NLR (see discussion in Dicken et al. 2009). Alternatively, if the illuminating AGN is highly variable and has recently 'switched on', the MIR continuum will be artificially enhanced relative to the emission from the NLR, because the compact nuclear dust structure ($r \sim 2$ pc according to our modelling) will respond more quickly to the change in AGN illumination than the larger-scale NLR ($r \sim 0.1$–1 kpc).

It is also interesting to consider the relationship between PKS 0043−42 and the other WLRGs in the 2-Jy sample. Along with the marked differences in the shape of its MIR continuum spectrum demonstrated in Fig. 1 and discussed in Section 2.1, PKS 0043−42 is 2–10 times more luminous at 24 μm than the other WLRGs at $z < 0.2$ (Dicken et al. 2009). Moreover, for the majority of these low-redshift WLRGs, the overall MIR continuum shape and extrapolation of the radio core continuum to MIR wavelengths suggest that a substantial fraction of their MIR continuum represents either synchrotron (Dicken et al. 2008) or thermal dust emission associated with starburst components (Leipski et al. 2009). Therefore, the position of most of the WLRGs close to the $L_{24\,\mu m}$ versus $L_{\rm [O III]}$ correlation derived for the 2-Jy sample as a whole (see fig. 6 in Dicken et al. 2009) may be misleading, since they would lie below the correlation if the synchrotron and the starburst contributions were subtracted. Indeed, there is no evidence for warm dust emission from a torus in the spectra of *any* of the $z < 0.2$ WLRGs in the 2-Jy sample apart from PKS 0043−42. If present, the torus component is likely to be substantially weaker in most WLRGs than it is in PKS 0043−42.

Overall, while PKS 0043−42 is likely to represent a low-luminosity counterpart of the SLRGs in terms of its nuclear structures and fuelling via cold accretion, such continuity in physical processes is unlikely to hold for many low-z WLRGs which show no evidence for warm dust emission associated with the torus. There-fore our results provide strong evidence that not all WLRGs are fuelled via the same mechanism.

REFERENCES

Allen S. W., Dunn R. J. H., Fabian A. C., Taylor G. B., Reynolds C. S., 2006, MNRAS, 372, 21
Antonucci R. R. J., 1993, ARA&A, 31, 473
Asensio Ramos A., Ramos Almeida C., 2009, ApJ, 696, 2075
Balmaverde B., Baldi R. D., Capetti A., 2008, A&A, 486, 119
Best P. N., Kaiser C. R., Heckman T. M., Kauffmann G., 2006, MNRAS, 368, L67
Bohlin R. C., Savage B. D., Drake J. F., 1978, ApJ, 224, 132
Buttiglione S., Capetti A., Celotti A., Axon D. J., Chiaberge M., Macchetto F. D., Sparks W. B., 2010, A&A, 509, 6
Decin L., Morris P. W., Appleton P. N., Charmandaris V., Armus L., Houck J. R., 2004, ApJS, 154, 408
Dicken D., Tadhunter C., Morganti R., Buchanan C., Oosterloo T., Axon D., 2008, ApJ, 678, 712
Dicken D., Tadhunter C., Axon D., Morganti R., Inskip K. J., Holt J., González Delgado R., Groves B., 2009, ApJ, 694, 268
Dicken D., Tadhunter C., Axon D., Robinson A., Morganti R., Kharb P., 2010, ApJ, 722, 1333
Elvis M. et al., 1994, ApJS, 95, 1
Ghisellini G., Celotti A., 2001, A&A, 379, L1
Hardcastle M. J., Evans D. A., Croston J. H., 2006, MNRAS, 370, 1893
Hardcastle M. J., Evans D. A., Croston J. H., 2007, MNRAS, 376, 1849
Hardcastle M. J., Evans D. A., Croston J. H., 2009, MNRAS, 396, 1929
Higdon S. J. U. et al., 2004, PASP, 116, 975
Houck J. R. et al., 2004, ApJS, 154, 18
Inskip K. J., Tadhunter C. N., Morganti R., Holt J., Ramos Almeida C., Dicken D., 2010, MNRAS, 407, 1739
Jaffe W. et al., 2004, Nat, 429, 47
Laing R. A., Jenkins C. R., Wall J. V., Unger S. W., 1994, in Bicknell G. V., Dopita M. A., Quinn P. J., eds, ASP Conf. Ser. Vol. 54, The Physics of Active Galaxies. Astron. Soc. Pac., San Francisco, p. 201
Lebouteiller V., Bernard-Salas J., Sloan G. C., Barry D. J., 2010, PASP, 122, 231
Leipski C., Antonucci R., Ogle P., Whysong D., 2009, ApJ, 701, 891
Lewis K. T., Eracleous M., Sambruna R. M., 2003, ApJ, 593, 115
Maiolino R., Marconi A., Salvati M., Risaliti G., Severgnini P., Oliva E., La Franca F., Vanzi L., 2001, A&A, 365, 28
Morganti R., Killeen N. E. B., Tadhunter C. N., 1993, MNRAS, 263, 1023

Morganti R., Oosterloo T. A., Reynolds J. E., Tadhunter C. N., Migenes V., 1997, MNRAS, 284, 541

Morganti R., Oosterloo T., Tadhunter C. N., Aiudi R., Jones P., Villar-Martín M., 1999, A&AS, 140, 355

Nenkova M., Ivezic Z., Moshe E., 2002, ApJ, 570, L9

Nenkova M., Sirocky M. M., Ivezic Z., Elitzur M., 2008a, ApJ, 685, 147

Nenkova M., Sirocky M. M., Nikutta R., Ivezic Z., Elitzur M., 2008b, ApJ, 685, 160

Nenkova M., Sirocky M. M., Nikutta R., Ivezic Z., Elitzur M., 2010, ApJ, 723, 1827

Ogle P., Whysong D., Antonucci R., 2006, ApJ, 647, 161

Packham C., Radomski J. T., Roche P. F., Aitken D. K., Perlman E., Alonso-Herrero A., Colina L., Telesco C. M., 2005, ApJ, 618, L17

Radomski J. T. et al., 2008, ApJ, 681, 141

Ramos Almeida C. et al., 2009, ApJ, 702, 1127

Ramos Almeida C., Tadhunter C., Inskip K. J., Morganti R., Holt J., Dicken D., 2011, MNRAS, 410, 1550

Roellig T. L. et al., 2004, ApJS, 154, 418

Sirocky M. M., Levenson N. A., Elitzur M., Spoon H. W. W., Armus L., 2008, ApJ, 678, 729

Tadhunter C. N., Morganti R., di Serego-Alighieri S., Fosbury R. A. E., Danziger I. J., 1993, MNRAS, 263, 999

Tadhunter C. N., Morganti R., Robinson A., Dickson R., Villar-Martín M., Fosbury R. A. E., 1998, MNRAS, 298, 1035

Tristram K. R. W. et al., 2007, A&A, 474, 837

Urry M., Padovani P., 1995, PASP, 107, 803

van der Wolk P. D., Barthel P. D., Peletier R. F., Pel J. W., 2010, A&A, 511, 64

This paper has been typeset from a TEX/LATEX file prepared by the author.